Derivation of the kinetics of devolatilisation and oxidation of pulverized biomass in a drop tube furnace: Sensitivity to volume evolution and drag-coefficient model

Hassan Mohanna, Jean-Michel Commandré, Bruno Piriou, Benoit Taupin, Gilles Vaitilingom, David Honoré

To cite this version:

Hassan Mohanna, Jean-Michel Commandré, Bruno Piriou, Benoit Taupin, Gilles Vaitilingom, et al.. Derivation of the kinetics of devolatilisation and oxidation of pulverized biomass in a drop tube furnace: Sensitivity to volume evolution and drag-coefficient model. Fuel, 2021, 293, pp.120434. ⟨10.1016/j.fuel.2021.120434⟩. ⟨hal-03539641⟩

HAL Id: hal-03539641

https://hal.science/hal-03539641v1

Submitted on 10 Mar 2023

Derivation of the kinetics of devolatilisation and oxidation of pulverized biomass in a drop tube furnace: Sensitivity to volume evolution and drag-coefficient model

Hassan MOHANNA[1-3], Jean-Michel COMMANDRE[1],
Bruno PIRIOU[1], Gilles VAITILINGOM[1], Benoit TAUPIN[2], David HONORE[3]
[1] CIRAD UPR BioWooEB, 34398 Montpellier, France
[2] Veolia Recherche et Innovation (VeRI), 78520 Limay, France
[3] Normandie Univ, INSA Rouen, UNIROUEN, CNRS, CORIA, 76000 Rouen, France

Abstract

Combustion experiments of raw and torrefied pine and demolition wood particles (600-800µm) are performed at 800°C in a drop tube furnace. The results provide the oxygen and carbon monoxide profiles along the reactor axis. These data are then used in a numerical model, developed to determine the kinetic parameters of devolatilisation and oxidation of the pulverized biomasses. In order to simulate the gas phase reactions, the model also takes as input the composition of the volatiles of the tested fuels measured during pyrolysis experiments at 800°C in the drop tube furnace. The model adopts different scenarios of particle volume evolution and different drag coefficient models in order to test their influence on the derived kinetic parameters. One of the volume evolution scenarios is a specific sub-model obtained by optical diagnostics of the combustion of the three biomasses in a previous study. Four other volume sub-models found in literature are also tested. For each of these scenarios, the model estimates close activation energy for devolatilization with a maximum variation of 2 $kJ \cdot mol^{-1}$ from one scenario to another, while the activation energy of char oxidation is more influenced, varying by 14 $kJ \cdot mol^{-1}$ with different scenarios. The five scenarios show similar gas concentrations and burnout versus the distance travelled by the particle. Nevertheless, this gives rise to a noticeable difference in the particle temperature along the furnace axis (±100°C at some positions), in addition to different particle velocity and residence time (~ ± 10%). The influence of the drag force is also studied using enhanced non-spherical model versus a spherical model. The non-spherical model leads to 10 to 14 $kJ \cdot mol^{-1}$ higher devolatilisation activation energies and 10 to 19 $kJ \cdot mol^{-1}$ higher char oxidation activation energies than the spherical model, along with a better prediction of the CO levels.

Nomenclature

A	Surface area (m^2)	t	Residence time (s)
Ac	Frequency factor for heterogeneous oxidation ($kg \cdot m^{-2}.s^{-1}.Pa^{-1}$)	T	Temperature (K)
Av	Frequency factor for devolatilization (s^{-1})	Ta	activation temperature (K)
C	Char content (kg of char · kg^{-1} of particles)	U	Unburnt fraction
C_D	Drag coefficient	v	Velocity ($m \cdot s^{-1}$)
Cp	Specific heat at constant pressure	V_p	Particle volume

D_{O2}	Mass diffusivity of oxygen ($m^2·s^{-1}$)	V	Volatiles content (kg of volatile matter · kg^{-1} of particles)
Dw	Mass diffusivity of water in the gas mixture ($m^2·s^{-1}$)	W	Moisture content (kg of water · kg^{-1} of particles)
dp	Particle diameter (m)	X_w	Water fraction in the gas phase
g	Gravitational acceleration (9.81 $m·s^{-2}$)	Sh	Sherwood number
E_c	Activation energy for heterogeneous oxidation ($kJ·mol^{-1}$)	λ	Thermal conductivity ($W·m^{-1}·K^{-1}$)
E_v	Activation energy for devolatilization ($kJ·mol^{-1}$)	τ	Particle relaxation time (s)
h	Coefficient of heat transfer convection	μ	Viscosity (kg · $m^{-1}·s^{-1}$)
H_c	Heat of heterogeneous combustion ($J·kg^{-1}$)	υ_c	Stoichiometric ratio of heterogeneous oxidation (kg O_2·kg C)
H_w	enthalpy of vaporization of water ($J·kg^{-1}$)	υ_i	Stoichiometric coefficient of oxidation reactions of volatile i (Kg species i· Kg^{-1} O2).
k_0	Frequency factor for volatiles reactions (s^{-1})	ρ	Density (kg · m–3)
k_c	Specific char oxidation rate ($kg.m^{-2}.s^{-1}$)	σ	Stefan–Boltzmann constant (5.67×10^{-8} $W·m^{-2}·K^{-4}$)
kdiff	Specific oxygen diffusion rate coefficient ($kg·m^{-2}·s^{-1}·Pa^{-1}$)	∅	Molar fraction of CO in the char oxidation reaction
Kv	Devolatilization rate (s^{-1})	ε	Particle emissivity
K_w	Moisture releasing rate (s^{-1})	*Subscripts*	
M	Molecular mass ($g.mol^{-1}$)	exp	Experimental value
n	Apparent reaction order	calc	Calculated value
N	Number of measured points	g	Free gas stream
Nu	Nusselt number	i	Volatile species (CO, CH_4, H_2)
P_{O2}	Partial pressure of oxygen (Pa)	p	Particle
Psat	Vapor saturation pressure (Pa).	r	Reactor
R	Universal gas constant ($J·mol^{-1}·K^{-1}$)	s	Particle surface
Re	Reynolds number	0	initial values at injection (t = 0)
Sc	The Schmidt number		

1. Introduction

With the increasing tendency of integrating biomass in combustion, a greater interest is given to acquire a detailed knowledge of the combustion phenomenon of biomass to improve the efficiency of combustion and evaluate its performance in pulverized combustion furnaces. In many ways, biomass is regarded as an economical solution of energy production and waste management. Its abundance and sustainability makes it a potential candidate of replacing some of the coal in the existing infrastructure.

Several coal power plants have been subject to cofiring projects and some even totally converted their consumption to biomass-derived fuels. Recently, Thunder Bay Unit 3 in Ontario [1] and Boardman power plant in Portland [2] entered service operating on 100% biomass instead of coal. Other power plants around the world are following the lead. The different physical and chemical properties of biomass make it difficult to project years' worth of accumulated research of coal directly on biomass. Studies have shown that even biochar or coal-like biomass obeys to completely different combustion behaviors than coal [3]. Therefore, it is necessary to extend our knowledge of the combustion of isolated biomass particles in order to validate the theoretical concepts describing the phenomena. This can provide detailed data, including kinetic parameters, to help the development of computational models, which can predict the behavior of biomass particles in industrial flames.

The combustion of coal and biomass particles at industrial and pilot scale studies are rarely available in the literature [4]–[10]. Rather, the research focuses mainly on lab-scale investigations to characterize the biomass. Drop tube furnace is one of the best methods to reproduce the realistic combustion conditions for isolated particles at high heating rate and short residence time. Specific sensors and direct observation techniques are used to access the degradation process of the particles in the hot gas stream. The data provides the combustion timeline, ignition delay, morphological evolution and pyrolysis products. Lu et al. [11] reported experimental data on the effect of particle shape on devolatilization of biomass in a drop tube furnace. Spherical particles lost mass slower than cylindrical ones, which in turn devolatilized slower than flake like particles. The study concluded to a more intense devolatilization as well as a higher degree of conversion for fine particles compared to coarser particles. The pyrolysis products were measured in several studies in drop tube furnace [12]. A very high gas yield is reported at high temperatures and heating rates. The main emitted species are CO_2, CO, H_2, CH_4, H_2O and heavier hydrocarbons with proportions dependent on the operating conditions and fuel type. CO is dominant at high temperatures, while hydrogen increases with it, and CO_2 tends to stabilize beyond 800°C [13]–[15].

Mathematical models have also been developed in a few studies to help data analysis to extract the kinetic parameters of devolatilization and char oxidation (*Table 1*), and subsequently predict other combustion parameters, as in Commandre et al. [16] for petcokes. Two approaches are proposed in this purpose: the model fitting approach and the 1D Lagrangian model. The first assumes that the combustion process in the DTF is performed by sections, each of them having its own set of kinetic parameters. Devolatilization occurs in the upper sections while char oxidation takes place in the lower sections. Costa et al. [17] applied this approach to determine the activation energies of the devolatilization and char oxidation of raw and torrefied pine shells ($Ev = 21.58\ kJ\cdot mol^{-1}$ – $Ec = 129.86\ kJ\cdot mol^{-1}$ and $Ev = 21.28\ kJ\cdot mol^{-1}$ – $Ec = 89.75\ kJ\cdot mol^{-1}$ respectively). In the same study, similar trends, but with much higher activation energies, were estimated for raw and torrefied olive stones. Using this approach, Farrow et al. [18] also obtained apparent activation energies between 24.2

kJ·mol^{-1} and 34.7 kJ·mol^{-1} for the pyrolysis of pinewood sawdust. On the other hand, Ballester and Jimenez [19] developed a detailed 1D Lagrangian model to perform numerical calculations on the particle thermal history based on the experimental data. The model was applied originally to coal and then adapted to biomass giving: Ev = 11 kJ·mol^{-1} and Ec = 63 kJ·mol^{-1} [20]. Wang et al. [21] also used this approach to evaluate the combustion behavior of biomass waste derived fuels, pine and coal in a drop tube furnace. Pereira et al. [22] applied both models to the combustion of poplar short rotation coppice. In comparison, the apparent activation energies in the devolatilization zone vary from 34.1 kJ·mol^{-1} for the model-fitting approach to 12.8 kJ·mol^{-1} for the detailed model proposed by Jiménez et al. [20], whereas in the char oxidation zone both models originate close apparent activation energies (73.2 kJ·mol^{-1} and 69.0 kJ·mol^{-1}). The distinct values are attributed to the simplifications considered in the model-fitting approach including the assumption of similar particle and gas temperature, which explains the higher activation energy of devolatilization, and the constant oxygen pressure at the particle surface along the furnace, which explains the higher activation energy of char oxidation.

Study	*Temperature (°C) – atmosphere – particle size*	*Fuel*	*Model approach*	*Av* (s^{-1})	*Ev* ($kJ·mol^{-1}$)	*Ac* ($g.m^{-2}.s^{-1}.Pa^{-1}$)	*Ec* ($kJ·mol^{-1}$)
Costa et al. [17]	*900, 950, 1000, 1050, 1100°C Air 30-1000µm*	*Raw pine*	*Model-fitting*	*0.3*	*21.6*	*1670.4*	*129.9*
		Torrefied pine		*0.4*	*21.3*	*54.9*	*89.8*
Farrow et al. [18]	*900, 1100, 1300, 1450 °C* *CO_2 and N_2* *125-250 µm*	*Pinewood*	*Model-fitting*	*63.4 - 100.1*	*24.2-34.7*	*-*	*-*
Pereira et al. [22]	*900, 950, 1000, 1050, 1100°C Air 20-1500 µm*	*poplar short rotation coppice*	*Model-fitting*	*5.1 x10^{-7}*	*34.1*	*0.05*	*73.2*
			1D Lagrangian	*90*	*12.8*	*0.38*	*69.0*
Jimenez and Ballester[20]	*1040, 1175, and 1300 °C* *Air* *100-1000 µm*	*Cynara cardunculus*	*1D Lagrangian*	*47.17*	*11*	*0.46*	*63*
Wang et al. [21]	*1100°C* *Air* *30-1128 µm*	*Pine braches*	*1D Lagrangian*	*15 x10^{3}*	*55*	*1.73*	*93*

Table 1: Survey of the kinetic parameters of devolatilization and oxidation of biomass using different model approaches

In this paper, we attempt to evaluate the combustion characteristics of raw and torrefied maritime pine and demolition wood in a drop tube furnace. Maritime pine is selected as a reference fuel for woody biomass as it is extensively studied in literature [17], [21], [23]–[26]. Demolition wood represents a resource of growing interest for energy production purposes. It is produced with large quantities in construction sites with no major technology to valorize it other than incineration [27]. A detailed combustion model uses the experimental data to determine the kinetic parameters of devolatilisation and oxidation of these fuels. In addition, it relies on the composition of the pyrolysis gas produced in pyrolysis experiments to model the gas phase reactions. Direct time-resolved observation and characterization of the combustion of these fuels, performed by particle combustion shadowgraphy in a previous study [3] provided the main scenario of the particle volume evolution. The latter is changed in the model to study the sensitivity of the obtained kinetic parameters on the volume scenario. The sensitivity study also addresses the influence of drag coefficient modeling on the calculation of the kinetic parameters.

2. Experimental setup

2.1 Biomass fuels

Maritime pine obtained from the south of France is used as a reference of raw biomass in this study (referred to as *Pine*). A part of the original biomass stock was torrefied at 280 °C for 25 min to produce particles with a lower volatile content (referred to as *Pint*). Demolition wood (*DW*) obtained from a demolished construction site was also used as representative of waste fuels. All of these fuels were first milled to a size range of 0 – 2 mm. The proximate and ultimate analyses of the fuels are listed in *Table 2* (following ASTM norm) alongside with the heating value and the aspect ratio (the ratio of the maximum length to the maximum width of the particle). Pine has a high moisture content, which is largely reduced by the torrefaction process generating pint. Torrefaction also reduces the volatile content while increasing the fixed carbon content and improving the energy density with higher heating value. Demolition wood has a chemical composition close to that of pine but with higher ash content due to the impurities contained within. This effect lowers its heating value.

	Maritime Pine (pine)	***Torrefied pine (pint)***	***Demolition wood (DW)***
Moisture	*11.46*	*1.93*	*6.32*
Ash (db)	*0.87*	*1.33*	*2.13*
Volatile matter (db)	*81.22*	*73.62*	*78.29*
Fixed carbon (db)	*18.58*	*25.05*	*19.57*
C (db)	*51.68*	*55.1*	*48.51*
H (db)	*5.93*	*5.68*	*5.63*
N (db)	*0.22*	*0.29*	*4.39*
O (db by difference)	*41.27*	*37.52*	*40.58*
LHV ($MJ\cdot kg^{-1}$) (db)	*18.45*	*19.73*	*17.71*
Aspect ratio	*2.50 ± 0.70*	*1.67 ± 0.40*	*2.08± 0.48*

Table 2: Fuels proximate and ultimate analysis and particles shape properties (db: dry basis)

The pulverized fuels were thoroughly sieved to a range of 600 - 800 µm. Pine particles are mostly flake-like while torrefied pine particles are mostly cylindrical and spherical. Demolition wood particles are mostly thick flakes made of small compressed fragments of wood [3].

2.2 Experimental setup

The drop tube furnace used in the present study is a heated reactor designed to reproduce the thermal conditions encountered in an industrial furnace with high heating rate. This experimental setup, located in the Rapsodee laboratory of Albi, France, was reconfigured for the purpose of this study (*Figure 1*). The apparatus is able to perform the study of biomass particles decomposition under various atmospheres (Air, N_2, etc.) and temperatures up to 1300°C. The achievable heating rates are in the order of 10^4 $°C \cdot s^{-1}$ [16]. The 1.5 m long reactor is an ø75mm alumina tube inside a three zones electric furnace covered with insulation fibers, and fed with an electrically preheated laminar gas flow. The solid fuel particles are injected in the reactor using the transport gas through a water-cooled feeding injector. At the end thereof, a 12 mm diameter stainless steel dispersion dome is held integral with the injector at a distance from the orifice of 1.2 mm. It disperses the fuel in an ideally homogeneous manner over the reactor cross-section. The primary gas and the particles are then mixed with the secondary gas flow inside the furnace. The thermal cycle of a particle begins at the moment it leaves the injection probe and immerses in the hot gas flow.

A sampling probe inserted through the outlet section permits sampling the gaseous effluents and solid particles at any height starting at 60 cm from the injection point. Indeed, previous temperature measurements indicated that the isothermal zone starts at 30 cm from the injector [15]. The probe is internally cooled by oil at 150 °C in order to quench the ongoing chemical reactions by a sudden decrease in the medium temperature and prevent the tars from condensing at the same time. Two-third of the total flow is sampled by the probe to ensure the collection of a representative sample. Subsequently, most of solid particles are collected in a bin at the bottom of the sampling probe, and the finest ones are trapped on a filter. Gases are then cooled in a condenser allowing to collect water and condensable species before conveying the dry gases to the analyzer via a set of heated lines.

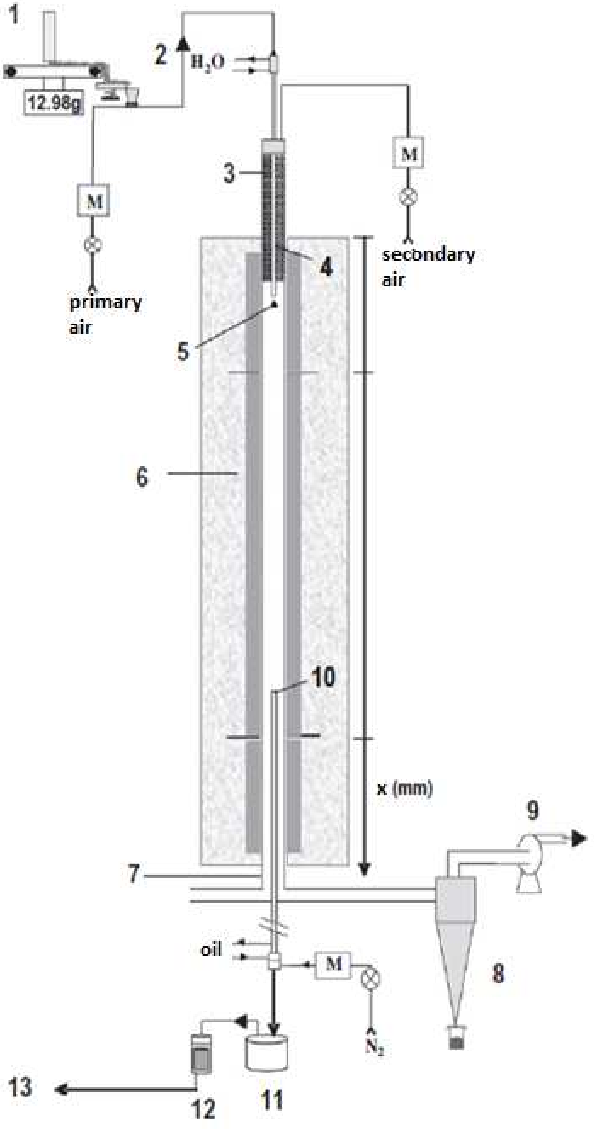

1. ***Controlled weighting system***
2. ***Pneumatic transport***
3. ***Electrical preheater***
4. ***Water cooled feeding probe***
5. ***Dispersion dome***
6. ***Three zone electrical furnace***
7. ***75mm i.d alumina tube reactor***
8. ***Cyclone collector***
9. ***Exhaust fan***
10. ***Oil cooled sampling probe***
11. ***Char pot***
12. ***Filter***
13. ***Gas analyzer***

M: Mass flow controller

Figure 1: Scheme of the drop tube furnace

2.3 Experimental procedures

In the view of the limitation set by the length of the sampling probe, the experimental conditions were chosen so that the biomass was not completely pyrolyzed upstream the first available sampling point, at 60 cm from the injection point, and reaches at the same time 80% conversion in combustion conditions at the final sampling point (150 cm). The temperature set point was the regulating parameter, since it is directly related to the conversion rate of the fuel. These conditions were achieved at a wall temperature of 800°C for biomass particles in the size range 600 to 800 µm.

The secondary airflow was preheated to the wall temperature before introducing it to the furnace. The solid fuel feeding rate was 1 g·min^{-1} transported by 2 l·min^{-1} (at STP) of primary airflow. The preheated gas flow was set to 20 l·min^{-1} (at STP) for all experiments. As observed from the bottom of the reactor, the biomass particles were falling in a single manner. Besides, the flow was highly diluted so that the particle-to-particle interactions can be neglected. In these conditions, the gas residence time inside the furnace was estimated to be 3.8 sec. The particle residence time during the combustion of a pine particle (600-800 µm) was estimated to be 0.674 sec using a physical model taking into consideration the size and density evolution of the particle and its slip velocity. During combustion, the conversion of the fuel as a function of the residence time was determined from the partial pressure of oxygen since the oxygen consumption is proportional to the burnout rate. This method is preferable over the ash tracer method, which leads to high uncertainty when dealing with low ash content solid fuels as explained by T. Ballantyne et al. [28], due to the uncertainty in the ash content measurement and the volatility of ash at high heating rates and temperatures. The concentrations of O_2 and CO were measured on line using a Testo gas analyzer model 350.

Moreover, experiments under pyrolysis conditions were performed in the purpose of quantifying the gas composition produced during the devolatilization stage of the particle. The gas composition is necessary to evaluate the gas phase reactions in the combustion model. The wall temperature was set to 800°C similarly to the combustion experiments. The particles were transported with nitrogen, which was also used as the secondary gas, preheated to the wall temperature. The gas was sampled at the exit of the reactor using sampling bags after being filtered and dried. The bags were then analyzed by a micro-GC to measure the mean concentrations of CO_2, CO, CH_4 and H_2 produced during the experiment.

3. Numerical modeling of the combustion of single biomass particles

A 1D Lagrangian model was coded on Matlab to perform numerical calculations on the particle thermal history based on the experimental data. The model allows the determination of the kinetic parameters of the physicochemical reactions that better reproduce the oxygen partial pressure obtained experimentally. Similar models have been proposed in [20] and [21], using also a 1D Lagrangian approach and similar kinetic formulation on thermally thin particles.

Main hypothesis

Considering the dilute particle flow in the experiments, the particle-to-particle interactions were neglected and the gas flow rate was considered constant at every point. Uniform temperature and homogeneous concentrations of chemical species are assumed in a horizontal section of the DTF.

The physical properties are described through the conservation equations of mass, momentum and energy exchange between a single particle and its surrounding environment. The devolatilization reaction and heterogeneous oxidation of char are described at the particle level.

The particle has a simplified composition, comprising only C, H, and O species. It has a spherical shape with the initial diameter equals to the average diameter of the sample.

Particle trajectory

In a gas-solid flow of particles in the studied size range, the drag and body forces are known to be the dominant forces. The velocity can be calculated by integrating the second law of motion:

$$m_p \frac{dv_p}{dt} = \frac{\pi d_p^2}{4} \cdot \frac{\rho_g}{2} \cdot C_D \left(v_g - v_p\right)^2 + m_p g - \rho_g V_p g \tag{1}$$

The Drag force, particle weight and Archimedes up-thrust are represented by the three terms on the right hand side. The drag coefficient C_D is expressed in the case of spherical particles by the Stokes law in terms of the Reynolds number:

$$\mathrm{C_D} = \frac{24}{Re_p} = \frac{24}{|v_g - v_p| \rho_g d_p / \mu} \tag{2}$$

Equation (1) can be rearranged in the following form:

$$\frac{dv_p}{dt} + \frac{1}{\tau}(v_g - v_p) = \left(\frac{\rho_g}{\rho_p} - 1\right) g \tag{3}$$

The right hand side is related to the buoyancy of the particle in the airflow. τ is the particle relaxation time given by the product of the particle mass and its mechanical mobility. This term characterizes the time required for the particle to adjust its velocity to a new condition of forces.

$$\tau = \frac{\rho_p V_p d_p}{12 \mu_g A_p} \tag{4}$$

Drying model

The drying process of the particle is modeled using the water diffusion approach [29]. The moisture flux contained in the particle increases with the particle temperature, which increases rapidly due to the high heating rate. The vapor release to the gas is controlled by the mass transfer between the surrounding gas and the particle.

$$\frac{dW}{dt} = 18 \cdot 10^{-2} \cdot K_w \left(\frac{P_{sat}}{RT_p} - \frac{X_w}{RT_g}\right) \tag{5}$$

With:

$$P_{sat} = 1.1 \cdot 10^{-5} \cdot exp\left[11 \cdot \left(T_p - 273.15\right)^{0.16}\right] \tag{6}$$

$$K_w = \left(2 + 0.6 \cdot Re_p^{1/2} Sc^{1/3}\right) \cdot \frac{D_w}{d_p} \tag{7}$$

Devolatilization and volatile combustion model

Literature shows that two competing steps devolatilization mechanisms are suitable for high heating rate pyrolysis modeling, but are more difficult to compute. As a first approach, we assume that the release rate of volatiles follows a one-step Arrhenius mechanism where Av and Ev are determined by iterations for the best match with experimental data.

$$\frac{dV}{dt} = A_v \cdot \exp\left(-\frac{E_v}{RT_p}\right).(V_0 - V) \tag{8}$$

The composition of the volatiles is determined by the pyrolysis experiments and it is assumed constant at all positions. The gas phase reactions are simplified to the oxidation reactions of the following combustible species: CO, H_2, and CH_4. The reactions are considered to be complete.

$$CO + \frac{1}{2} O_2 \rightarrow CO_2 \tag{9}$$

$$H_2 + \frac{1}{2} O_2 \rightarrow H_2O \tag{10}$$

$$CH_4 + 2O_2 \rightarrow CO_2 + 2H_2O \tag{11}$$

The reactions rate R_i, is formulated under the Arrhenius form where ρ_{aj} (in kmol·m^{-3}) is the molar density of the species a_j. The parameters are given in *Table 3*.

$$R_i = k_{0,i} exp\left(\frac{T_{a,i}}{T}\right).T^{b0} \rho_{a1}^{b1} \rho_{a2}^{b2} \rho_{a3}^{b3} \tag{12}$$

Reaction i	**$k_{0,i}$**	**$T_{a,i}$**	**b0**	**a1**	**b1**	**a2**	**b2**	**a3**	**b3**
1	$1 \cdot 10^{+15}$	16000	-1.5	CO	1	O_2	0.25	H_2O	0.5
2	$5.16 \cdot 10^{+13}$	3430	-1.5	H_2	1.5	O_2	1	-	-
3	$3.55 \cdot 10^{+12}$	15700	-1	CH_4	1	O_2	1	-	-

Table 3: Values to be used for computations of gas-gas reaction rates [30]

Char oxidation model

The heterogeneous char oxidation starts once oxygen reaches the particle surface and reacts with carbon atoms. The reaction produces CO and CO_2 with a temperature dependent ratio ($0 < \emptyset < 1$) [14].

$$C + \left(1 - \frac{\emptyset}{2}\right) O_2 \rightarrow \emptyset CO + (1 - \emptyset) CO_2 \tag{13}$$

$$R_c = \frac{[CO]}{[CO_2]} = 2500 \cdot \exp\left(-\frac{51843}{RT_p}\right) = \frac{\emptyset}{1-\emptyset} \tag{14}$$

Therefore, the rate of the oxidation depends on the diffusion rate of oxygen and the chemical reaction rate.

$$\frac{dC}{dt} = -A_p k_c P_{O_2,s}^n \tag{15}$$

kc is the chemical reaction rate coefficient. $P_{O_2,s}$ is the oxygen partial pressure at the particle surface supplied by molecular diffusion, which obeys Fick's law:

$$\dot{m}_{O_2} = \pi d_p Sh D_{O_2} \frac{M_{O_2}}{RT_g}(P_{O_2,g} - P_{O_2,s}) \tag{16}$$

Sherwood number (Sh) was set to 2 by assumption. Note that the effect of the outward flow of the species is negligible and the supplied oxygen by diffusion is consumed by the heterogeneous reaction. After arranging the above equations and setting n to unity [20], the carbon consumption can be rewritten as follows:

$$\frac{dC}{dt} = -A_p \frac{1}{\frac{1}{K_{diff}} + \frac{1}{K_c}} P_{O_2,g} \tag{17}$$

The diffusion and chemical kinetic coefficients are calculated:

$$K_{diff} = Sh.v_c \frac{D_{O_2}}{d_p} \frac{M_{O_2}}{RT_g} \quad (18); \qquad k_c = A_c \cdot \exp\left(-\frac{E_c}{RT_p}\right) \quad (19)$$

The remaining volatiles and char form the unburnt fraction U of the particle. The evolution of the particle volume was obtained for each biomass in a previous study from direct observation and characterization of the particle degradation by optical diagnostics in [3] assuming that particles are spherical and isotropic.

$$d_p = d_{p_0} f(U) \tag{20}$$

$$U = \frac{C + (V_0 - V)}{C_0 + V_0} \tag{21}$$

Where $f(U)$ is a characteristic function of each fuel type in terms of the unburnt fraction. Assuming spherical particles and isotropic consumption, the particle volume can be directly evaluated from its projection area. In fact, the initial particle shape was fibrous and irregular for all types. The irregularities tend to disappear in the remaining char, which becomes more rounded than the original particle [31], [32]. The high temperatures encountered during the char combustion allow the particle to deform and smooth the edges.

Heat balance

The particle temperature is different from the gas and wall temperatures. The small size of the particle limits the temperature gradient within the particle, so they can be considered thermally thin in our operating conditions [33] as Biot number is low. The heat balance can be converted into the following equation by assuming that mixing between atmosphere gas and transport gas is instantaneous [16]:

$$C_{pp} m_p \frac{dT_p}{dt} = h_p A_p \left(T_g - T_p\right) + A_p \varepsilon \sigma \left(T_r^4 - T_p^4\right) - \frac{dW}{dt} \cdot H_w - \frac{dC}{dt} \cdot f_h H_C - \sum \dot{m}_i C_{pi} T_p \tag{22}$$

Once introduced in the furnace, the particle is exposed to convection with the surrounding gas and to radiation from the furnace wall represented by the first and second terms in the right hand side. Particle absorption of energy during drying is accounted for by the third term, while the fourth term includes the energy released during char combustion. f_h being the coefficient of heat release from char combustion due to incomplete combustion.

$$f_h = 1 - 1.44 \cdot \left(1 - \frac{12}{32} \cdot \frac{1}{v_c}\right) \tag{23}$$

The particle energy balance does not include a heat exchange term between the particle and the flame. Instead, we assume that the flame heats up the surrounding gas, which in turn heats the particle. The assumption is backed experimentally by the observations made by Riaza et al. [34] in a visual free fall reactor, where a perfectly spherical flame envelops the particle at a lift-off distance. The last term of heat balance represents the heat fluxes supplied to the environment by the gases leaving the particle. During their ejection, the volatiles exchange heat with the particle, as well as with the gas phase. The ejected volatiles also exchange heat with the stream gas by convection, before liberating their energy through oxidation, causing a temperature rise in the gas phase. The energy balance of the gas phase is formulated as follows:

$$C_{pg} \dot{m}_g \frac{dT_g}{dt} = h_p A_p \left(T_p - T_g\right) + h_r A_r \left(T_r - T_g\right) + \sum R_i \cdot H_i + \sum \dot{m}_i C_{pi} T_p \tag{24}$$

The terms in the right hand side include respectively: the convection heat transfer between the particle and the gas, the convection heat transfer between the furnace wall and the gas, the liberated heat from the oxidation of the volatiles, and the heat fluxes supplied to the environment by the gases leaving the particle. The Nusselt number of convection between the gas phase and the reactor inner wall is determined by Mill's model for convection in a vertical cylinder [35].

Derivation of kinetic parameters

Oxygen is involved in the main chemical reactions occurring in the furnace. Therefore, $P_{O2,g}$ is not constant and its evolution should be followed to provide the input parameters for the particle consumption. A relationship is established between the partial pressure of oxygen and the consumed volatiles and char to determine its value at a given position x.

$$P_{O_2,x} - P_{O_2,0} = \frac{\rho_g R T_g}{M_{O_2}} \cdot \frac{Q_f}{Q_g} \cdot \left(\sum_i \frac{1}{\upsilon_i} \cdot V_i + \frac{1}{\upsilon_c} \cdot (C_0 - C)\right) \qquad (25)$$

The first term in the right hand side sums the contribution of the oxidation reaction of each volatile species. Vi represents each species of the volatiles (CO, H_2, CH_4) and υ_i is the corresponding stoichiometric coefficient of the oxidation reaction (Kg species i· Kg^{-1} O_2). Oxygen consumed by the char is represented by the second term.

The prediction is compared with the measured oxygen content (%vol.) along the furnace axis. The deviation between both values is calculated:

$$\delta = \sum \frac{1}{N} \cdot \left([O_2]_{exp} - [O_2]_{calc}\right)^2 \qquad (26)$$

The code runs in iterations in two rounds to spot the optimal pairs of kinetic parameters (Av, Ev) and (Ac, Ec) providing the best prediction by minimizing the deviation function δ. *Table 4* presents the scanned ranges and the increment values of each parameter.

	Av **($1 \cdot s^{-1}$)**	**Ev** **($kJ \cdot mol^{-1}$)**	**Ac** **($g \cdot m^{-2}.s^{-1}.Pa^{-1}$)**	**Ec** **($kJ \cdot mol^{-1}$)**
First run				
Range	1-500	1-100	0.01-5	1-100
Increment	1	0.5	0.01	0.5
Second run				
Range	Av1 ± 10	Ev1 ± 0.5	Ac1 ± 0.1	Ec1 ± 0.5
Increment	1	0.1	0.01	0.1

Table 4: The scanned ranges of the kinetic parameters

The code runs a first round in these ranges to spot (Av1, Ev1) and (Ac1, Ec1). A second run is done in a more refined range around the values spotted in the first round with a smaller increment.

4. Results and discussion

4.1 Preliminary pyrolysis experiments

The pyrolysis of biomass decomposes the lignocellulosic components into light gases, tar, and char. Tar eventually breaks down into light hydrocarbons. The gaseous species are mainly composed of CO, CO_2, H_2, CH_4 and a small proportion of heavier hydrocarbons such as C_2H_4, C_2H_6. The pyrolysis gas composition (% by mass) from pine, pint and DW are presented in *Figure 2*. These compositions of the pyrolysis gas of each fuel are used in the numerical model when simulating their combustion.

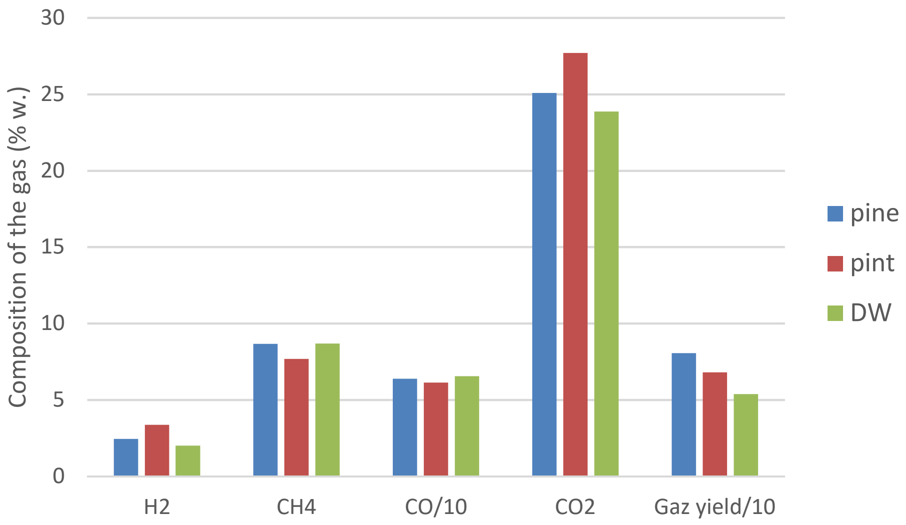

Figure 2: Comparison of the pyrolysis gas composition for different biomasses at 800°C (fuel size 600-800µm)

The higher moisture content in pine (11.46%) did not reduce the gas yield in front of the low moisture pint. Indeed, an investigation on the fast pyrolysis of pine with different moisture content (10.7% versus 0% (dried)) in [15], at 850°C for 0.9 to 1.5 s under nitrogen, concluded that the natural moisture has no influence on the amount and nature of the final pyrolysis gas. While the overall gas yield of pine is typical to what has been reported for the flash pyrolysis of wood in similar conditions [36]–[38], demolition wood has low gas yield. This may be due to its higher density, which increases its velocity and reduces the residence time in the reactor. Torrefied pine ejected less volatiles during the experiment with lower CO and CH_4 yields. CO was quantified as the major fraction of the produced gases followed by CO_2, CH_4 and H_2 respectively. This is in line with previous studies [39], [40]. The high percentage of oxygen in the biomass favors the formation of CO. The µ-GC also detected peaks corresponding to C_2H_2, C_2H_2 and C_2H_6 but they were not quantified. Heavier hydrocarbons were not detected in the analysis. They may have appeared earlier in the conversion pathway of volatiles, but cracked to methane, hydrogen and soot through polymerization and reformation.

4.2 Combustion

4.2.1 Kinetic parameters

The biomass fuels were injected at 800 °C with a sufficient airflow rate so that the oxygen fraction at the furnace exit is at least of 16%. The model iteratively minimizes the difference between the calculated and measured concentration of oxygen to determine the kinetic parameters. *Figure 3* compares the predicted and the measured evolutions of the oxygen partial pressure on dry basis along the reactor longitudinal axis corresponding to the three tested fuels. The algorithm successfully follows the experimental points leaving a very low error margin. *Table 5* lists the kinetic parameters with the corresponding deviations from the experimental points. The values are close to those reported elsewhere using a similar model, for the devolatilization and char oxidation of raw and torrefied pine shell in [17] and of Cynara cardunculus in [20].

	Av *($1\cdot s^{-1}$)*	***Ev*** *($kJ\cdot mol^{-1}$)*	***Ac*** *($g\cdot m^{-2}.s^{-1}.Pa^{-1}$)*	***Ec*** *($kJ\cdot mol^{-1}$)*	***δ*** *eq.(26)*
Pine	294	18.3	0.93	53	$1.6\cdot 10^{-04}$
Pint	107	19.0	1.65	65	$1.7\cdot 10^{-03}$
DW	380	21.0	3.70	53	$3.1\cdot 10^{-03}$

Table 5: Kinetic parameters obtained by the mathematical model for the tested fuels

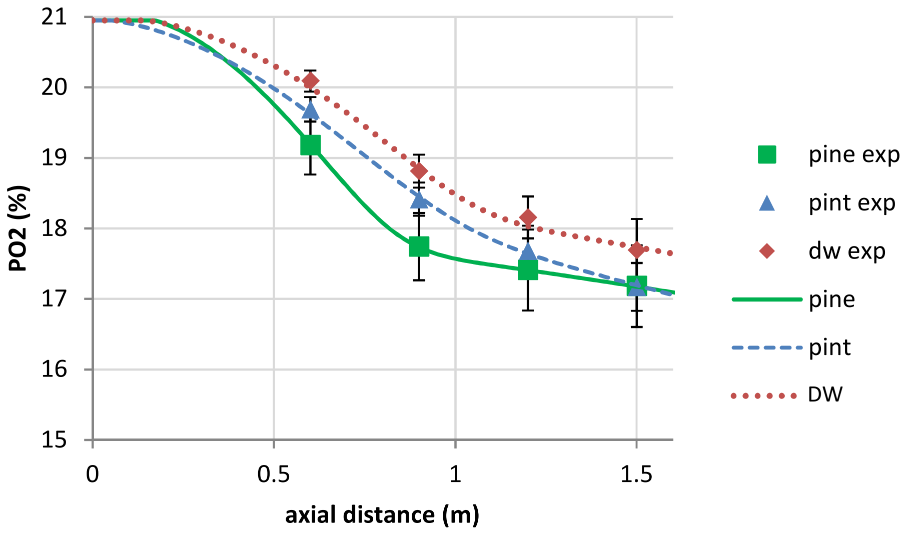

Figure 3: Evolution of %O_2 partial pressure along the tube furnace axis (600 – 800 µm particles at 800°C with air)

However, a detailed DTF-model by Wang et al. [21] similar to this study, calculated activation energies for five other biomasses, two to three times higher than the values calculated here. The difference is however compensated by a very high pre-exponential factor ($15 - 300 \cdot 10^3$ s^{-1}), but still, the model showed large discrepancies between measurements and predictions in the near injector zone where most of the devolatilization takes place. It should be noted that the experimental conditions were different in [21] (see *Table 1*), and the combustion air was injected at room temperature and consequently the particles are exposed to a different heating rate. This probably induces the different combustion kinetics. Another factor creating this difference between the models predictions is their corresponding particle volume evolution that will be discussed later. Therefore, based on this review, the activation energies in *Table 5* are in accordance to what can be found in literature using similar models and experimental conditions.

The results show that higher activation energies are calculated for demolition wood than pine. Moreover, torrefaction reduces the reactivity of devolatilization and char oxidation which is consistent with previous studies [41].

4.2.2 Particle conversion

The first sampling point at 60 cm from the injection point marks some oxygen consumption observed for the three fuel types. Upstream this point, the model predicts the combustion parameters based on their measured tendencies later. At this distance, the particles have already started their degradation journey, which is estimated to last for 0.674 sec for pine, 0.772 sec for pint, and 0.572 sec for DW inside the furnace. The heating rate is around 2000°C·s^{-1} as calculated by the model.

After injection, particle temperature increases until around 100°C during the release of moisture from the particle. Most of the received energy at this stage is absorbed as latent heat for drying and thus the particle temperature stabilizes for a certain time as simulated in *Figure 4*. Demolition wood and pine with roughly 6 % and 11 % moisture content respectively experience a significant delay in initiation of their devolatilization compared to the relatively dry particles (~ 2% moisture) of torrefied pine. The latter takes advantage for an early increase in temperature. No oxygen is consumed during the drying stage. Drying is directly followed by a rapid liberation of volatiles associated with high consumption rate of oxygen. Despite the late start, pine leads the consumption rate given the low activation energy and the more intense devolatilization pointed out in a previous study [3]. The heavier demolition wood particles acquire higher speeds than pine and pint and thus devolatilize over a longer axial distance, which explains their smoother oxygen consumption as well as smoother temperature rise during this phase. Oxygen consumption slows down at the end of devolatilization and the beginning of the char combustion. By now, the particle temperature comes closer to the furnace temperature but does not reach it yet, due to the high thermal inertia of the coarse particles. Subsequently, the particles are heated by the char oxidation, and then cools down after full consumption until they reach equilibrium with the ambient conditions at 800 °C. Simulations with finer particles reveal faster heating to the extent they overpass the furnace temperature during the flame phase.

The conversion profiles (*Figure 5*) are calculated using the derived optimal kinetic parameters. The model indicates that most of the biomass particle journey is devoted for devolatilization due to high volatile content, and the influence of char conversion is marginal on the total burnout. Given the obtained data, on the basis of our previous work [3] on particle combustion shadowgraphy at 800°C in air, it was also possible to calculate the overlap between the homogenous and heterogeneous combustion stages. The flame extinction is assumed when 99.9 % of the initial volatile content is released, whereas the heterogeneous ignition is the moment when 0.1 % of the initial FC is consumed.

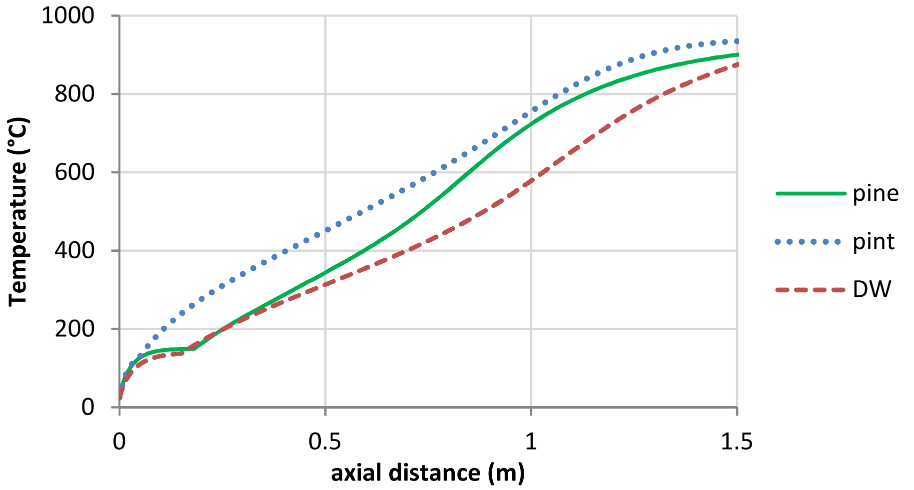

Figure 4: The predicted particle temperature along the furnace axis (600 – 800 µm particles at 800°C with air)

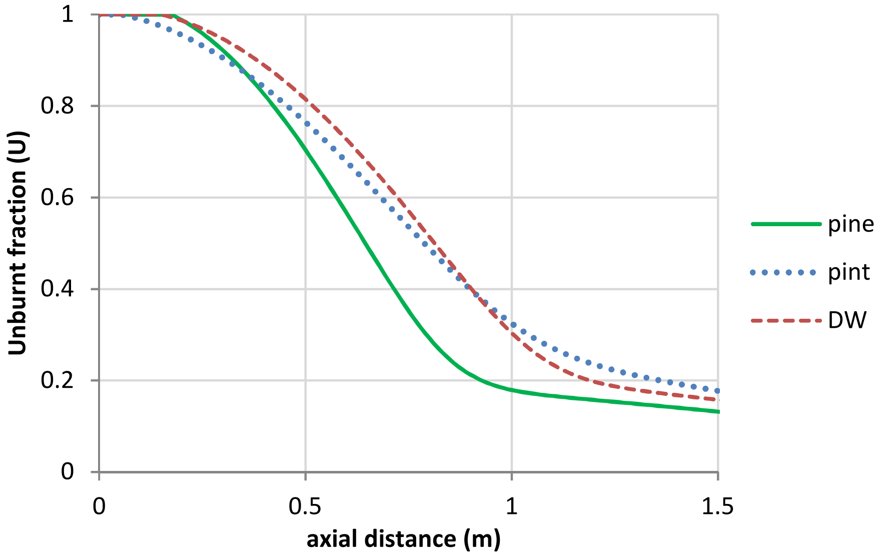

Figure 5: The predicted unburnt fraction of the studied fuels (600 – 800 µm particles at 800°C with air)

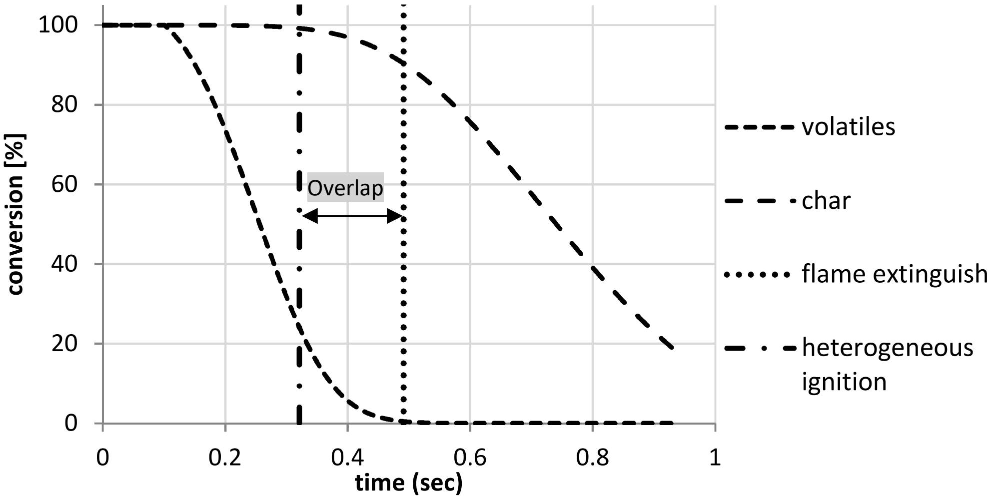

Figure 6: overlap of the flame phase and char combustion phase during DW combustion (600 – 800 µm particles at 800°C with air)

Figure 6 illustrates this method applied for the combustion of demolition wood. The maximum overlap was obtained for torrefied pine (0.217 sec), followed by demolition wood (0.161 sec) and the minimum overlap for pine (0.097 sec). These durations are somehow longer than the measured ones in [3] for such particle size. Nevertheless, the arrangement of the overlap durations is consistent. Given similar particle size, the overlap is mainly affected by the volatile matter content and the intensity of devolatilization, leading to pine-DW-pint series from lower to higher overlap duration.

4.2.3 Volatiles oxidation

Figure 7 shows the prediction and the experimental data of the CO molar fraction along the reactor axis. In comparison to the experimental results, CO is overestimated during devolatilization at 60 cm but then better fits to the experimental data during char combustion. The overestimation may be related to the fact that CO was calculated based on a constant composition of volatiles that was measured during the pyrolysis experiments. The good prediction of CO validates the model, given that the CO experimental measurements were not used for the determination of the kinetic parameters.

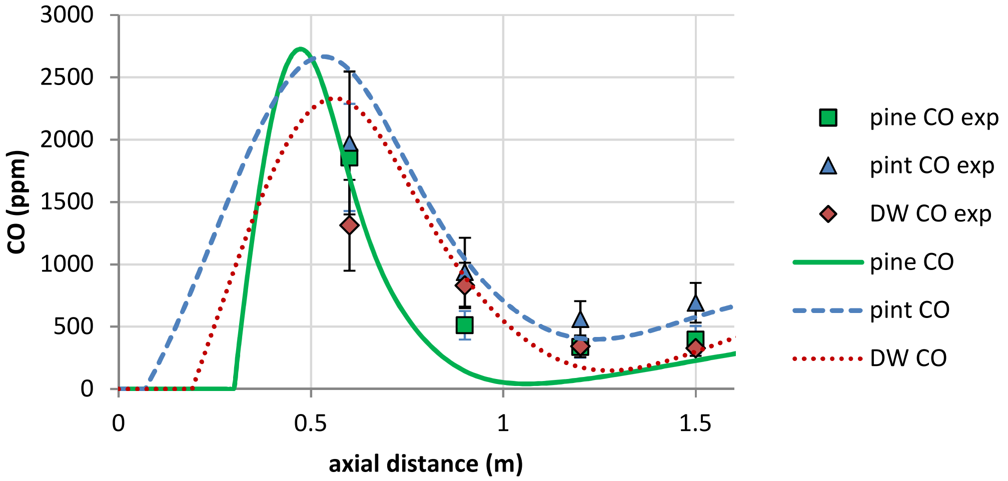

Figure 7: Evolution of CO concentration along the tube furnace axis for pine, pint and DW combustion (600-800µm particles at 800°C with air)

The behavior is quite similar for the three fuel types. CO is produced in high concentrations during devolatilization forming a peak before the first sampling point. This peak is directly related to the peak of devolatilisation. Despite its delayed start, pine exhibits earlier peak followed by pint and DW. The concentration then decays upon oxidation and with lower devolatilisation rate. The release of moisture promotes the early activation of the CO oxidation reaction and the earlier decay of CO, especially in the case of pine. CO decay continues to the point where char is ignited and CO emerges again as the major product of the char oxidation reaction at high temperatures. The value of the attained minimum reflects the degree of overlap between the combustion stages. In the case of pine, CO approaches zero before the second rise, while higher value of the local minimum is reached by DW and pint respectively, despite the lower production in the flame phase. This also can be observed from the tendencies of the experimental points.

4.2.4 Sensitivity study

*4.2.4.1 **Influence of the volume evolution model***

This section discusses the sensitivity of the model predictions to the volume evolution scenario of the particle. As discussed earlier, previous studies used similar approaches but employed simplified volume evolution scenarios. They are listed from # 1 to # 4 in *Table 6*, our proposal is labelled # 0.

Scenario	*Flame phase*	*char combustion*
#0	*Experimental data from* [3]	*Experimental data from* [3]
#1	*Constant volume*	*Shrinking core (α=0.33)*
#2	*Constant volume*	*Constant volume*
#3	*Swelling model*	*Shrinking core (α=0.25)*
#4	*Swelling model*	*Constant volume*

Table 6: Volume evolution scenarios of a biomass particle during each combustion stage

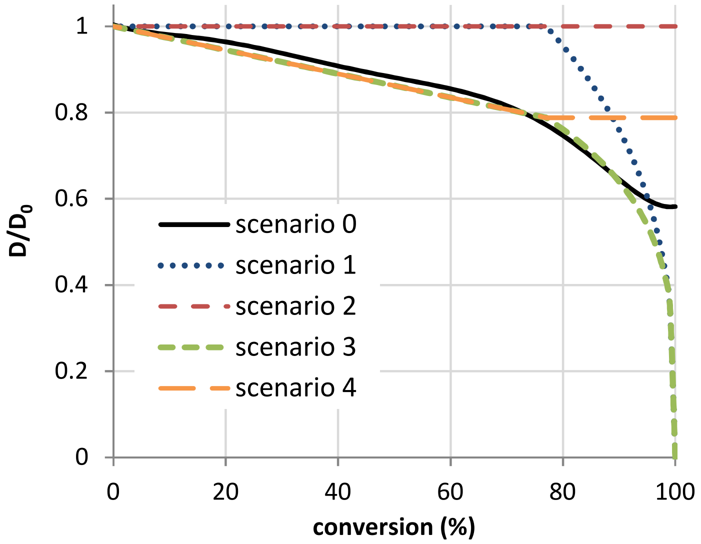

Figure 8: Volume evolution scenarios of a biomass particle versus its conversion during combustion

Wang et al. model in [21] did not take into account the variation of the particle volume during devolatilization assuming constant volume, but a shrinking core was considered during char oxidation (scenario 1). On the other hand, based on experimental data, Jimenez et al. [20] assumed a constant volume for the particles in the course of their combustion (scenario 2), taking into account a density variation. This assumption is also used for coal in some studies [42]. However, many CFD studies adopt different volume evolution scenarios based on works initially developed for coal: the swelling particle model for devolatilization is often adapted to biomass by setting the swelling coefficient smaller than one. Using intrinsic model for the char oxidation part, a shrinking core model with 0.25

power coefficient has been found to work well for a variety of chars (scenario 3) [43]. However, most CFD studies use a kinetic/diffusion char surface oxidation model with constant particle diameter (scenario 4). *Figure 8* shows the five scenarios of diameter evolution during the combustion of pine.

A direct comparison of the parameters obtained in these studies may not be objective, considering that they were applied on different fuel types and experimental conditions. The four volume evolution scenarios from literature were tested here, in addition to our volume model obtained by particle combustion shadowgraphy (scenario 0). The char conversion is not well established in our experiments, so the simulation is extended to allow comparison until the complete burnout.

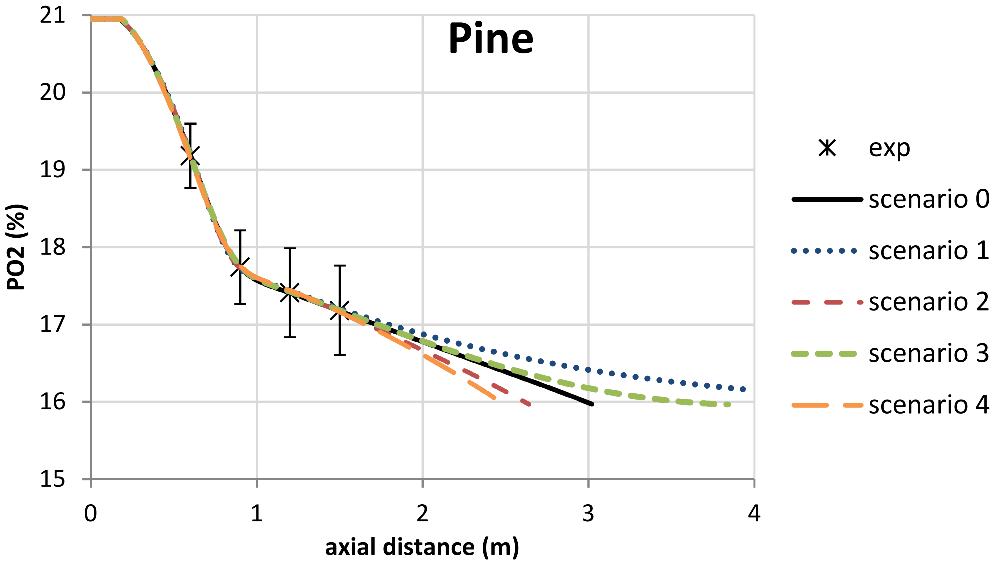

Figure 9: Model fitting of oxygen curves to the pine experimental points using different scenarios. The axial distance is extended beyond the furnace length to allow comparison at higher conversion.

Figure 9 shows the model fitting of oxygen partial pressure to the experimental points, using the optimal parameters determined for each case. The curves agree up to the last experimental point, but they diverge afterwards in the absence of experimental data at higher conversion. In order to better judge and compare the results of each case, the model should have the same data input to follow until the complete burnout. Therefore, the oxygen pressure calculated in scenario 0, based on the available experimental points, is taken as a baseline input for the other scenarios. In this case, the model optimizes the oxygen curve of each scenario to reproduce the curve determined in scenario 0.

Table 6 summarizes the kinetic parameters of each fuel in each volume evolution case. The kinetics of scenario 0 and scenario 3 are very similar as expected, since their volume models stick together up to a high conversion point. For all scenarios, the values of devolatilization kinetics are comparable considering the same mathematical formulation. Moreover, the impact of shrinkage is negligible on the pyrolysis time and yield in such regime [44]. The one-step reaction is not directly dependent on the particle volume. The volume rather influences the velocity and temperature, which are not fully established after injection.

	Av ($1\cdot s^{-1}$)	*Ev* ($kJ\cdot mol^{-1}$)	*Ac* ($g\cdot m^{-2}.s^{-1}.Pa^{-1}$)	*Ec* ($kJ\cdot mol^{-1}$)
Pine				
Scenario0 (this study)	294	18.3	0.93	53
Scenario1	220	17	1.50	67
Scenario2	230	17	0.40	60
Scenario3	290	17.8	1.4	53.4
Scenario4	290	17.2	0.51	53
Non-spherical drag (SF=0.25)	248	27.4	0.92	63.5
Pint				
Scenario0	107	19	1.65	65
Scenario1	118	20	3.30	75
Scenario2	122	20	0.78	67
Scenario3	107	19	2.10	65
Scenario4	102	18.5	0.90	61
Non-spherical drag (SF= 0.33)	250	32.4	2.11	72
DW				
Scenario0	380	21	3.70	53
Scenario1	435	22	1.20	59
Scenario2	435	22	0.84	61
Scenario3	430	21.5	2.51	53.7
Scenario4	371	20	0.53	51
Non-spherical drag (SF =0.25)	331	30	3.40	70

Table 7: Comparison of the kinetic parameters due to the model sensitivity to volume evolution

The difference for these entities (velocity in *Figure 10* and temperature in *Figure 11*) appears after the first 50 cm where devolatilization has already started. Afterwards, a reduced volume pushes the particle faster due to lower drag force. Hence, the volatiles in scenarios 0, 3 and 4 are released over a wider distance so they get more diluted and their oxidation is less intense. Whereas in scenarios 1 and 2, the particles spend more time in intense volatile combustion region, which favors their temperature rise. Ultimately, the particles have longer residence time in the furnace in these scenarios 1 and 2 (~+10% longer) and higher average temperature. The calculations are then performed at lower temperature during the char oxidation for scenarios 0, 3 and 4 (around 100°C lower), and by following the same burnout data, it means that char oxidation is activated at lower temperature, which explains the lower activation energy. It is evident how the algorithm is sensitive to the evolution of the particle size during this stage, because it is directly linked to the consumption rate.

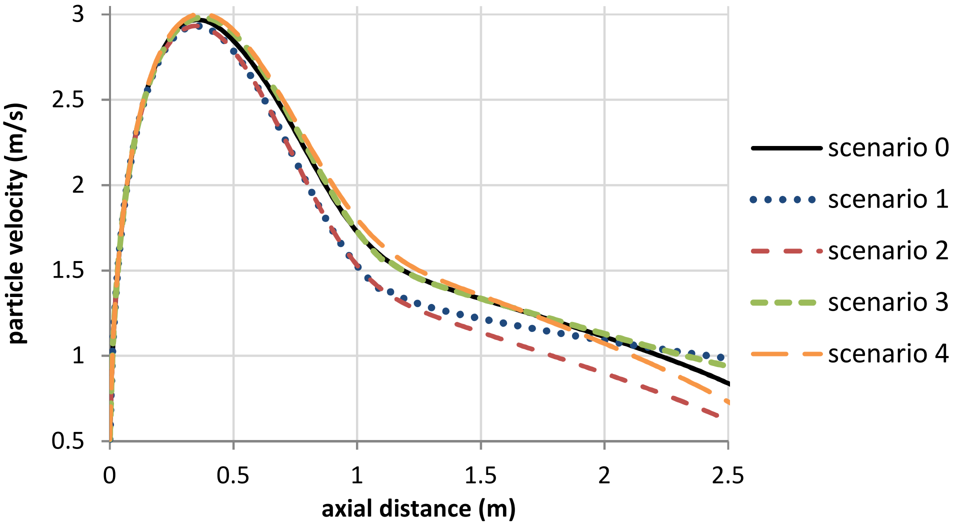

Figure 10: Sensitivity of the particle velocity to the volume evolution model (pint- (600 – 800 µm) at 800°C with air)

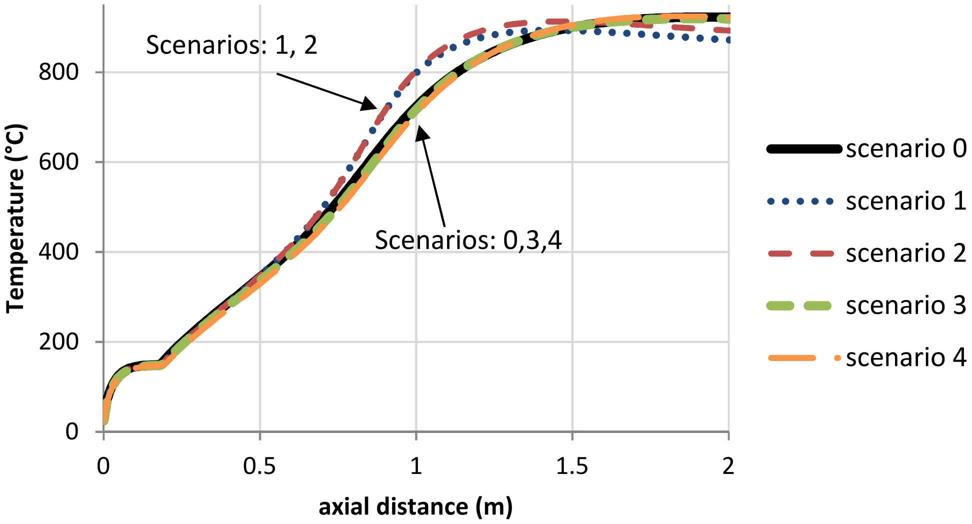

Figure 11: Sensitivity of particle temperature to the volume evolution model (pine (600 – 800 µm) at 800°C with air)

Changing the particle volume not only affects the chemical kinetics but also affects the diffusion of oxygen pressure to the particle surface. The diffusion kinetics is firstly controlled by the particle and gas temperature, and secondly, by the oxygen pressure in the surrounding gas. Faster particles devolatilize over a wider distance and thus oxygen consumption is slightly smoother. In this case (scenarios 0, 3 and 4), before the end of the flame where it starts to shrink back to the particle surface, the particle is surrounded by slightly higher oxygen pressure than in the other scenarios. This promotes the oxygen diffusion and consequently helps triggering the heterogeneous reaction. This also explains the longer overlap duration of homogeneous and heterogeneous reactions for scenario 0, 3 and 4 in all three fuels types resulting in the series: scenario4 > scenario0 > scenario3 > scenario1 > scenario2.

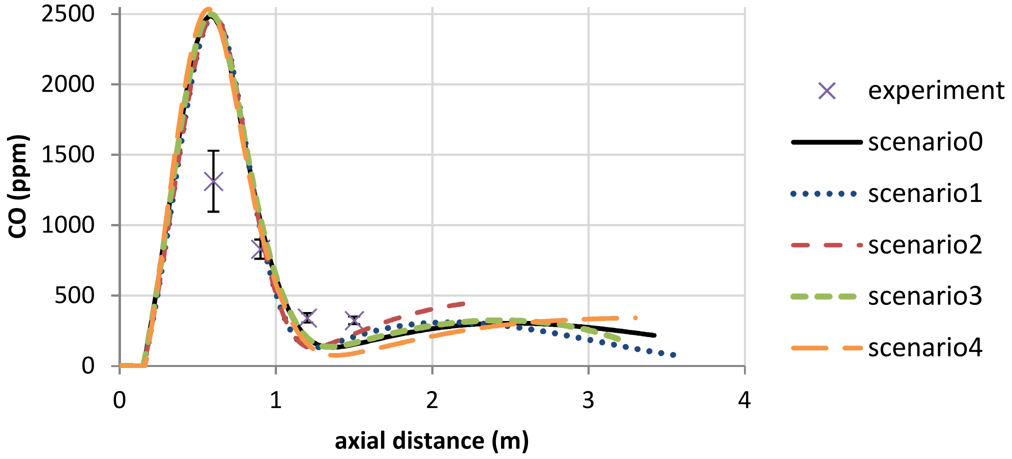

Figure 12: CO sensitivity to the volume evolution model (DW (600 – 800 µm) at 800°C with air), The axial distance is extended beyond the furnace length to allow comparison at higher conversion

The predictions of CO concentration (*Figure 12*) and burnout using different scenarios do not change dramatically when traced versus the axial distance; since the model in all cases follow the experimental points at a certain position which does not refer to the same residence time in every scenario. Given close apparent kinetics for devolatilization, it is normal for the profiles not to show high variations at this stage. The differences appear more pronounced during char oxidation where the consumption rate varies with the scenario. The kinetics are faster with lower activation energy and attain higher conversion within shorter residence time.

4.2.4.2 Influence of the drag force model

The disparity of the values of the kinetic parameters found in literature results from different used sub-models. Each has some impact on the particle trajectory and/or its thermal history. With the same given burnout data, the models are compelled towards different optimal kinetic values in order to better predict the experimental data. Modeling drag coefficient is very critical to determining the particle trajectory. Considering the uncertainty of the particle initial shape and its change during the degradation process, modeling the drag coefficient is a difficult task requiring simplified approaches. The model adopted in this study is the simplest approach as it treats particles as spherical and ignores the shape evolution in the course of their conversion. In fact, particles with arbitrary shapes are shown to be exposed to a higher drag force compared to the equivalent spherical particles [45], [46]. Several correction methods are proposed in order to include the effect of non-sphericity on the drag force.

In the present study, the kinetic parameters are recalculated alongside the particle thermal and conversion history, using the non-spherical model proposed by Haider and Levenspiel [47]. Scenario 4 is employed for the volume evolution. The model is a function of the shape factor (SF) of the particle, which is defined as the ratio of the surface area of a sphere-equivalent particle (with the same volume), to the actual surface area of the particle. *Table 6* shows the kinetic parameters of devolatilization and char combustion of the three fuels using the non-spherical drag law. The chosen shape factors are used as surveyed in the literature for raw and torrefied wood [45], [46], [48]–[50]. Torrefied biomass is found to have higher SF due to its lower fiber content compared to raw biomass.

Figure 13 traces the influence of the drag coefficient modeling on the particle velocity. Particles with non-spherical shape are exposed to high drag effect forcing them to advance slowly in the combustion chamber. This effect is true for all fuel types. The velocity peak of a spherical particle is more than twice faster than the non-spherical one. Consequently, the improved interaction of the random shape particle with the flow gives a faster temperature rise near the injection point (*Figure 14*). Water is released in shorter distance allowing the temperature to increase further. However, the initiation of devolatilization is interpolated from the same data points fed to both models. Therefore, the non-spherical particles are supposed to devolatilize at higher temperature. This shift is translated to higher activation energy as seen in *Table 6*.

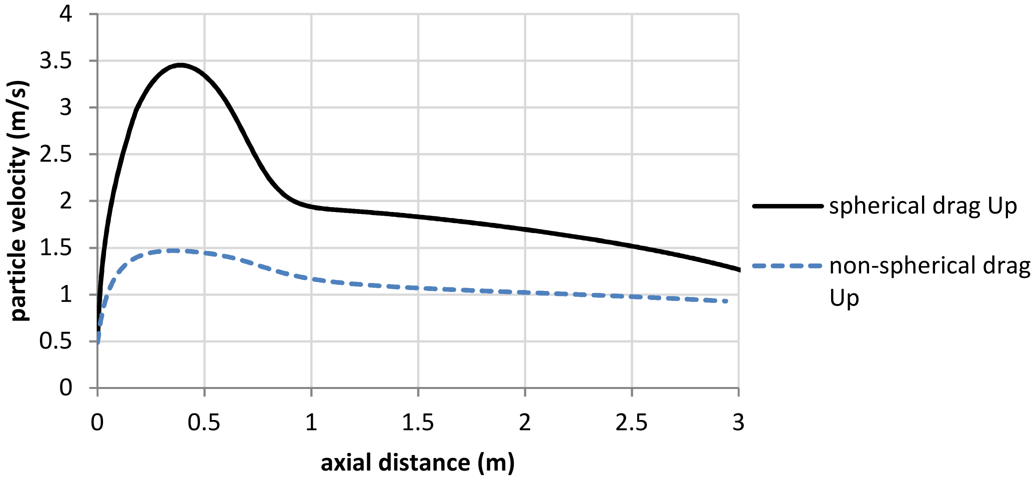

Figure 13: Influence of drag modeling on the particle velocity (pine (600 - 800 µm) at 800°C with air)

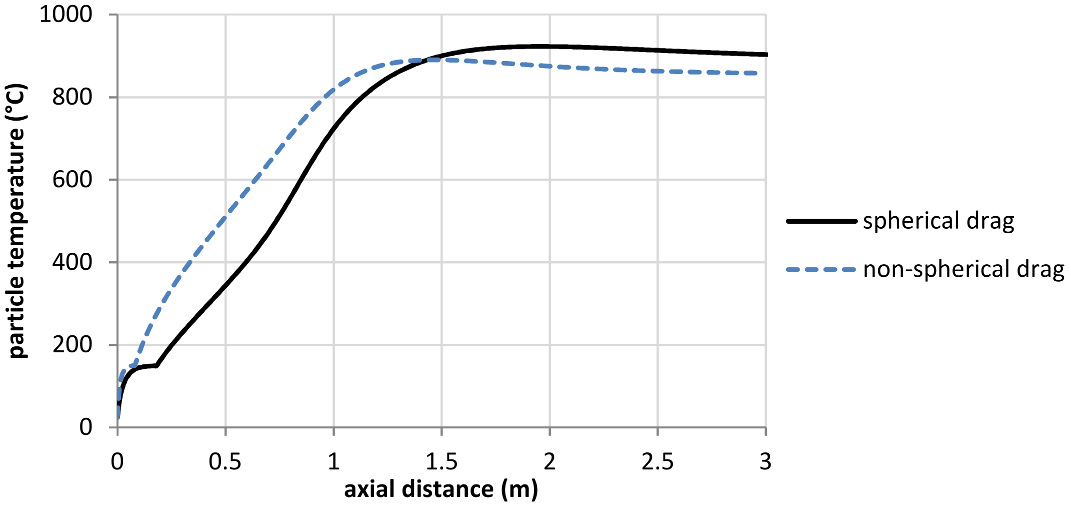

Figure 14: Influence of drag modeling on the particle temperature (pine (600 – 800 µm) at 800°C with air)

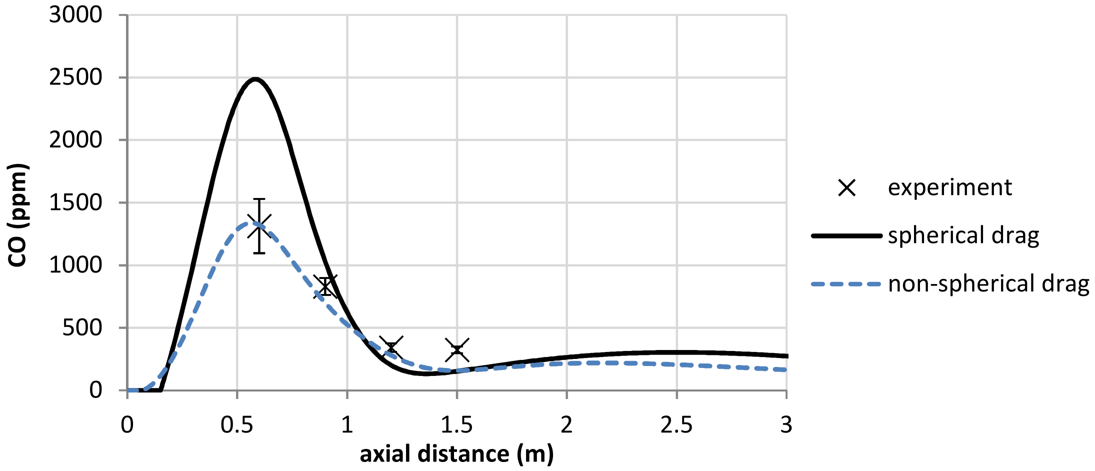

Figure 15: Influence of drag modeling on the concentration of CO along the furnace axis. (DW (600 – 800 µm) at 800°C with air)

The modified trajectory of the particle also influences the distribution of volatiles in the combustion chamber. A slow-moving particle releases its volatiles over a shorter distance. This intensifies the reaction rate of oxidation of the volatiles leaving lower concentrations of CO. *Figure 15* presents the comparison of the two drag models with the experimental measurements of CO during the combustion of demolition wood. Accounting for the non-sphericity of the particle reproduces better the experimental data of CO.

5. Conclusion

The combustion of raw and torrefied pine and demolition wood particles is studied in a drop tube furnace at 800°C. In order to determine the kinetic parameters of devolatilization and char oxidation of each fuel, this study proposes a numerical model using both the pyrolysis gas composition measured during preliminary pyrolysis experiments and an empirical sub-model developed specifically to describe the volume evolution of a single particle observed at 800°C [3]. The model proposed in the present study predicts well the oxygen and carbon monoxide concentrations, consistent with the literature. However, the kinetic values of char oxidation are lower than those reported in similar studies. This can be related to different experimental conditions, and is partly due to the differences in model approaches, especially considering the volume evolution and the drag coefficient of the particles. Four other scenarios of the particle volume evolution found in literature are used, to evaluate how dependent the kinetic parameters are on the volume sub-model. Our previous study using particle combustion shadowgraphy generates very close kinetics to those found using a swelling and shrinking scenario during devolatilization and char oxidation respectively. However, when assuming a constant particle volume during devolatilization, the model converges to the experimental points with higher activation energy. The four scenarios simulate similarly the gas concentrations and burnout versus the distance travelled by the particle. Nevertheless, this has to be considered with caution considering the difference in the particle temperature along the furnace axis, in addition to different particle velocities and residence time. The Influence of drag coefficient model is also addressed in this study. The model compares the kinetic parameters obtained using enhanced non-spherical model of drag versus those obtained using a spherical model. The former model gives higher activation energies for devolatilization (10 to 14 $kJ \cdot mol^{-1}$ higher) and char oxidation (10 to 19 $kJ \cdot mol^{-1}$ higher), and better predicts the CO levels. The particle combustion model and the obtained kinetic parameters in this study will be integrated in a CFD model of biomass flames in a pilot scale reactor.

Acknowledgments

The authors acknowledge the help of S. Salvador for the access to the entrained flow reactor at Ecole des Mines Albi. This work is financially supported by the ANRT (Convention CIFRE - N° 2016/0523).

References

[1] "Ontario Power Generation, Canada Coal to biomass journey furnace," Ontario, Canada, 2018.

[2] U. Nowling, "Successful Torrefied Biomass Test Burn at a Coal Power Plant," 2018.

[3] H. Mohanna, J.-M. Commandre, B. Piriou, G. Vaitilingom, B. Taupin, and D. Honore, "Shadowgraphy investigation of the combustion of raw and pre-treated single biomass particles: Influence of particle size and volatile content," *Fuel*, vol. 258, p. 116113, Dec. 2019.

[4] R. Weber, T. Kupka, and K. Zając, "Jet flames of a refuse derived fuel," *Combust. Flame*, vol. 156, no. 4, pp. 922–927, Apr. 2009.

[5] R. Weber, Y. Poyraz, A. M. Beckmann, and S. Brinker, "Combustion of biomass in jet flames," *Proc. Combust. Inst.*, vol. 35, no. 3, pp. 2749–2758, 2015.

[6] A. Elfasakhany, L. Tao, B. Espenas, J. Larfeldt, and X. S. Bai, "Pulverised wood combustion in a vertical furnace: Experimental and computational analyses," *Appl. Energy*, vol. 112, pp. 454–464, Dec. 2013.

[7] J. Li, E. Biagini, W. Yang, L. Tognotti, and W. Blasiak, "Flame characteristics of pulverized torrefied-biomass combusted with high-temperature air," *Combust. Flame*, vol. 160, no. 11, pp. 2585–2594, Nov. 2013.

[8] D. Ristic *et al.*, "Development of a pilot-scale flameless oxidation burner for ultra-low NOx combustion of pulverised coal," 2008.

[9] M. Weidmann *et al.*, "Experimental characterization of pulverized coal MILD flameless combustion from detailed measurements in a pilot-scale facility," *Combust. Flame*, vol. 168, pp. 365–377, Jun. 2016.

[10] S. S. Daood, M. T. Javed, A. H. Rizvi, and W. Nimmo, "Combustion of Pakistani Lignite (Thar Coal) in a Pilot-Scale Pulverized Fuel Down-Fired Combustion Test Facility," *Energy & Fuels*, vol. 28, no. 2, pp. 1541–1547, Feb. 2014.

[11] H. Lu, E. Ip, J. Scott, P. Foster, M. Vickers, and L. L. Baxter, "Effects of particle shape and size on devolatilization of biomass particle," *Fuel*, vol. 89, no. 5, pp. 1156–1168, May 2010.

[12] S. Zellagui *et al.*, "Pyrolysis of coal and woody biomass under N 2 and CO 2 atmospheres using a drop tube furnace - experimental study and kinetic modeling," *Fuel Process. Technol.*, vol. 148, pp. 99–109, Jul. 2016.

[13] C. Dupont, J.-M. Commandré, P. Gauthier, G. Boissonnet, S. Salvador, and D. Schweich, "Biomass pyrolysis experiments in an analytical entrained flow reactor between 1073K and 1273K," *Fuel*, vol. 87, no. 7, pp. 1155–1164, Jun. 2008.

[14] J.-M. Commandré, "Formation des oxydes d'azote lors de la combustion de cokes de pétrole dans des conditions de précalcinateur de cimenterie," L'Institut National Polytechnique de Toulouse, 2002.

[15] J.-M. Commandré, H. Lahmidi, S. Salvador, and N. Dupassieux, "Pyrolysis of wood at high temperature: The influence of experimental parameters on gaseous products," *Fuel Process. Technol.*, vol. 92, no. 5, pp. 837–844, May 2011.

[16] J.-M. COMMANDRÉ, S. SALVADOR, L. VAN DE STEENE, and R. GADIOU, "The Formation and Reduction of NO During The Combustion of Petroluem Coke- The case of Cement Plant Precalciner Condtions," *Combust. Sci. Technol.*, vol. 177, no. 3, pp. 579–611, Feb. 2005.

[17] F. F. Costa, G. Wang, and M. Costa, "Combustion Kinetics and Particle Fragmentation of Raw and Torrified pine shells and olive stones in a Drop Tube Furnace," *Proc. Combust. Inst.*, vol. 35, no. 3, pp. 3591–3599, 2015.

[18] T. S. Farrow, C. Sun, and C. E. Snape, "Impact of CO2 on biomass pyrolysis, nitrogen partitioning, and char combustion in a drop tube furnace," *J. Anal. Appl. Pyrolysis*, vol. 113, pp. 323–331, May 2015.

[19] J. Ballester and S. Jiménez, "Kinetic parameters for the oxidation of pulverised coal as measured from drop tube tests," *Combust. Flame*, vol. 142, pp. 210–222, 2005.

[20] S. Jiménez, P. Remacha, J. C. Ballesteros, A. Giménez, and J. Ballester, "Kinetics of devolatilization and oxidation of a pulverized biomass in an entrained flow reactor under realistic combustion conditions," *Combust. Flame*, vol. 152, no. 4, pp. 588–603, Mar. 2008.

[21] G. Wang, R. B. Silva, J. L. T. Azevedo, S. Martins-Dias, and M. Costa, "Evaluation of the combustion behaviour and ash characteristics of biomass waste derived fuels, pine and coal in a drop tube furnace," *Fuel*, vol. 117, pp. 809–824, Jan. 2014.

[22] S. Pereira, P. C. R. Martins, and M. Costa, "Kinetics of Poplar Short Rotation Coppice Obtained from Thermogravimetric and Drop Tube Furnace Experiments," *Energy & Fuels*, vol. 30, no. 8, pp. 6525–6536, Aug. 2016.

[23] A. Dhaundiyal and J. Gangwar, "Kinetics of the thermal decomposition of pine needles," *Acta Univ. Sapientiae, Agric. Environ.*, vol. 7, no. 1, pp. 5–22, Dec. 2015.

[24] N. Gao, A. Li, C. Quan, L. Du, and Y. Duan, "TG–FTIR and Py–GC/MS analysis on pyrolysis and combustion of pine sawdust," *J. Anal. Appl. Pyrolysis*, vol. 100, pp. 26–32, Mar. 2013.

[25] J. Zhao, S. Niu, Y. Li, K. Han, and C. Lu, "Thermogravimetric Analysis and Kinetics of Combustion of Raw and Torrefied Pine Sawdust," *J. Chem. Eng. Japan*, vol. 48, no. 4, pp. 320–325, 2015.

[26] E. Rodriguez Alonso, C. Dupont, L. Heux, D. Da Silva Perez, J.-M. Commandre, and C. Gourdon, "Study of solid chemical evolution in torrefaction of different biomasses through solid-state 13C cross-polarization/magic angle spinning NMR (nuclear magnetic resonance) and TGA (thermogravimetric analysis)," *Energy*, vol. 97, pp. 381–390, Feb. 2016.

[27] "Les quantités de déchets produits et éliminés en France en 2004," 2004.

[28] T. R. Ballantyne, P. J. Ashman, and P. J. Mullinger, "A new method for determining the conversion of low-ash coals using synthetic ash as a tracer," *Fuel*, vol. 84, no. 14–15, pp. 1980–1985, Oct. 2005.

[29] D. SHIN and S. CHOI, "The Combustion of Simulated Waste Particles in a Fixed Bed," *Combust. Flame*, vol. 121, pp. 167–180, 2000.

[30] M. De Souza-Santos, *Solid Fuels Combustion and Gasification Modeling, Simulation, and Equipment Operations*, Second edi. New York: Taylor & Francis Group, 2010.

[31] A. Panahi, Y. A. Levendis, N. Vorobiev, and M. Schiemann, "Direct observations on the combustion characteristics of Miscanthus and Beechwood biomass including fusion and spherodization," *Fuel Process. Technol.*, vol. 166, pp. 41–49, Nov. 2017.

[32] C. Meesri and B. Moghtaderi, "Experimental and numerical analysis of sawdust-char combustion reactivity in a drop tube reactor," *Combust. Sci. Technol.*, vol. 175, no. 4, pp. 793–823, Apr. 2003.

[33] K. M. Bryden, K. W. Ragland, and C. J. Rutland, "Modeling thermally thick pyrolysis of wood,"

Biomass and Bioenergy, vol. 22, no. 1, pp. 41–53, Jan. 2002.

[34] J. Riaza *et al.*, “Combustion of single biomass particles in air and in oxy-fuel conditions,” *Biomass and Bioenergy*, vol. 64, pp. 162–174, May 2014.

[35] R. S. Subramanian, “Heat transfer in Flow Through Conduits,” 2014.

[36] J.-M. Commandré, H. Lahmidi, S. Salvador, and N. Dupassieux, “Pyrolysis of wood at high temperature: The influence of experimental parameters on gaseous products,” *Fuel Process. Technol.*, vol. 92, no. 5, pp. 837–844, May 2011.

[37] L. Chen, “Fast pyrolysis of millimetric wood particles between 800°C and 1000°C,” Lyon 1, 2009.

[38] L. Wei *et al.*, “Characteristics of fast pyrolysis of biomass in a free fall reactor,” *Fuel Process. Technol.*, vol. 87, no. 10, pp. 863–871, Oct. 2006.

[39] D. Neves, A. Matos, L. Tarelho, H. Thunman, A. Larsson, and M. Seemann, “Volatile gases from biomass pyrolysis under conditions relevant for fluidized bed gasifiers,” *J. Anal. Appl. Pyrolysis*, vol. 127, pp. 57–67, Sep. 2017.

[40] S. Septien, S. Valin, C. Dupont, M. Peyrot, and S. Salvador, “Effect of particle size and temperature on woody biomass fast pyrolysis at high temperature (1000–1400°C),” *Fuel*, vol. 97, pp. 202–210, Jul. 2012.

[41] P. McNamee, L. I. Darvell, J. M. Jones, and A. Williams, “The combustion characteristics of high-heating-rate chars from untreated and torrefied biomass fuels,” *Biomass and Bioenergy*, vol. 82, pp. 63–72, Nov. 2015.

[42] R. Lewtak and J. Hercog, “COAL CHAR KINETICS OF OXIDATION AND GASIFICATION REACTIONS,” *Chem. Process Eng.*, vol. 38, no. 1, pp. 135–145, 2017.

[43] I. W. Smith, “The kinetics of combustion of pulverized semi-anthracite in the temperature range 1400–2200°K,” *Combust. Flame*, vol. 17, no. 3, pp. 421–428, Dec. 1971.

[44] K. M. Bryden and M. J. Hagge, “Modeling the combined impact of moisture and char shrinkage on the pyrolysis of a biomass particle☆,” *Fuel*, vol. 82, no. 13, pp. 1633–1644, Sep. 2003.

[45] M. Mandø, L. Rosendahl, C. Yin, and H. Sørensen, “Pulverized straw combustion in a low-NOx multifuel burner: Modeling the transition from coal to straw,” *Fuel*, vol. 89, no. 10, pp. 3051–3062, Oct. 2010.

[46] L. Ma, J. M. Jones, M. Pourkashanian, and A. Williams, “Modelling the combustion of pulverized biomass in an industrial combustion test furnace,” *Fuel*, vol. 86, no. 12–13, pp. 1959–1965, Aug. 2007.

[47] A. Haider and O. Levenspiel, “Drag coefficient and terminal velocity of spherical and nonspherical particles,” *Powder Technol.*, vol. 58, no. 1, pp. 63–70, May 1989.

[48] Palo Sidwell Pokothoane, “Analysis of co-firinf of biomass with South African coal in pulverised coal boilers.,” University of the Witwatersrand, 2010.

[49] N. Niemelä, “Computational fluid dynamics modeling of pulverized biomass combustion using optimized reactivity paramaters,” Tampere University of Technology, 2015.

[50] R. C. R. Lima, R. F. B. Gonçalves, Manoel F. M. Nogueira, and Danielle R. S. Guerra, “Simulation study of biomass powder combustion in cyclonic furnace,” in *23rd ABCM International Congress of Mechanical Engineering*, 2015.